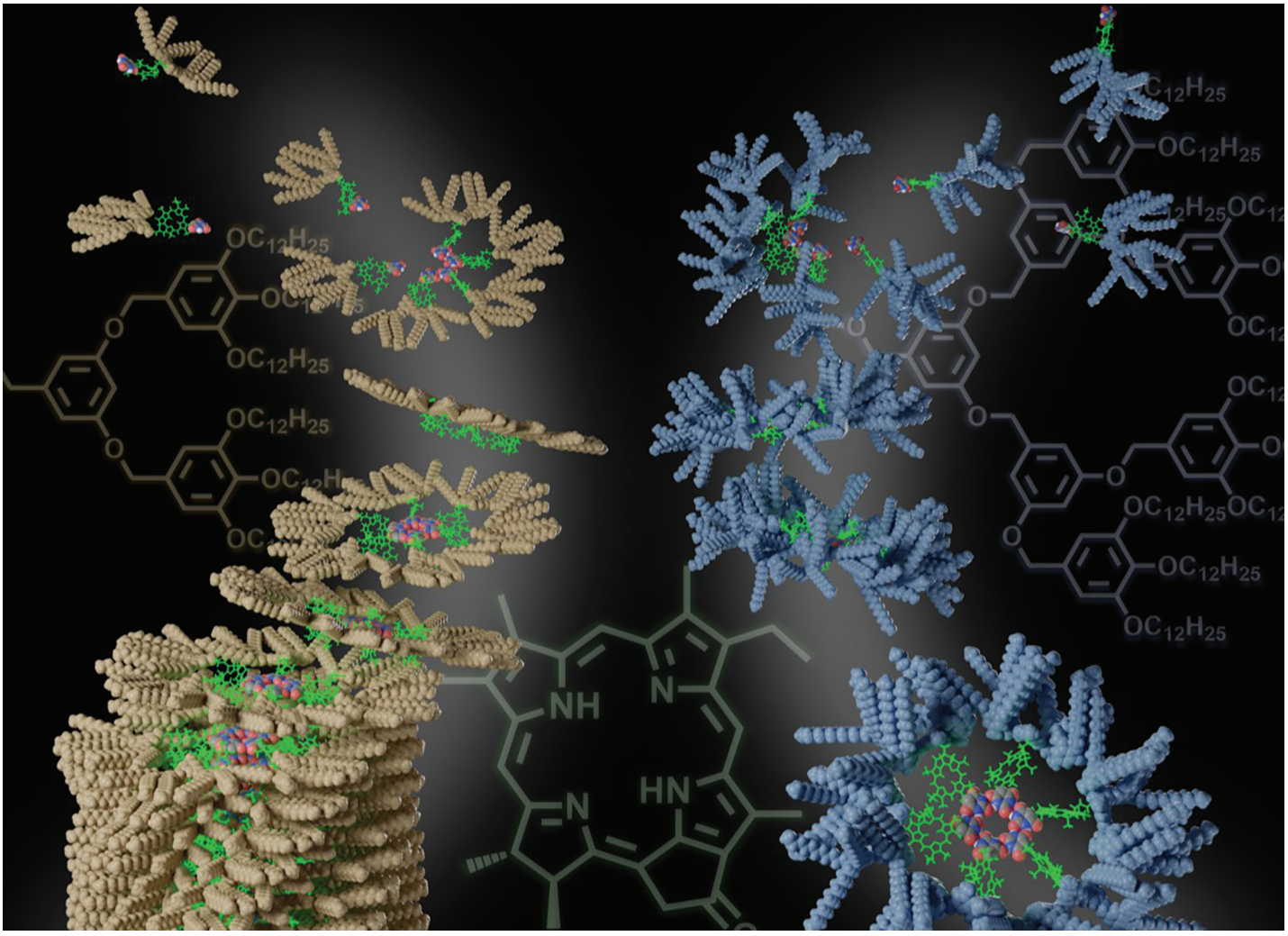


**Showcasing research from Professor Shiki Yagai's laboratory, Division of Advanced Science and Engineering, Graduate School of Engineering, Chiba University, Chiba, Japan.**

Dendron-mediated control over self-assembly of chlorophyll rosettes into columnar *vs.* discrete aggregates

By controlling the π–π stacking of chlorophyll supramolecular rosettes through steric hindrance of alkyl dendrons, it becomes possible to create chlorophyll tubes and discrete rings that resemble natural chlorophyll assemblies.

As featured in:

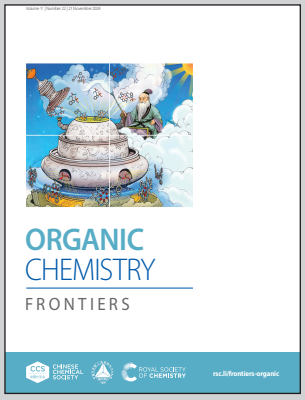


See Shiki Yagai *et al.*, *Org. Chem. Front.*, 2024, **11**, 6304.



CCS 中国化学会 CHINESE CHEMICAL SOCIETY
SIOC 1950
ROYAL SOCIETY OF CHEMISTRY
rsc.li/frontiers-organic

ORGANIC CHEMISTRY FRONTIERS

CCS 中国化学会 CHINESE CHEMICAL SOCIETY

SIOC 1950

ROYAL SOCIETY OF CHEMISTRY

RESEARCH ARTICLE

View Article Online
View Journal | View Issue



Cite this: *Org. Chem. Front.*, 2024, **11**, 6304

# Dendron-mediated control over self-assembly of chlorophyll rosettes into columnar *vs.* discrete aggregates†

Ryo Kudo,[a] Hiroki Hanayama,[b] Balaraman Vedhanarayanan,[c] Hitoshi Tamiaki,[d] Nobuyuki Hara,[d,e] Sarah E. Rogers,[f] Martin J. Hollamby,[g] Biplab Manna,[h] Koji Harano[h,i] and Shiki Yagai *[b,j]

Received 3rd September 2024,
Accepted 5th October 2024

DOI: 10.1039/d4qo01629g

rsc.li/frontiers-organic

Photosynthetic bacteria have evolved highly efficient light-harvesting systems by organizing chlorophyll (Chl) pigments into circular and tubular supramolecular arrays. To construct these surapmoelcular Chl arrays from the same molecular design, we synthesized two hydrogen-bonding chlorins using natural Chl-*a* as the starting material: free-base chlorin functionalized with hydrogen-bonding barbituric acid and second- or third-generation alkyl dendrons (G2 and G3, respectively). The barbituric acid moiety promotes the formation of a hydrogen-bonded cyclic hexamer known as rosette. In chloroform, both the synthetic Chl-*a* derivatives formed rosettes; however, in methylcyclohexane as a low-polarity solvent, the G2-dendron chlorin formed columnar structures by stacking rosettes, while the G3-dendron chlorin formed disc-shaped particles. AFM revealed the formation of extended helical fibers for the former and homogeneous nanoparticles, possibly single rosettes, for the latter. These results suggest that the third-generation of the dendron can inhibit the stacking of rosettes, leading to the formation of two distinct types of chlorin aggregates: circular and tubular.



## Introduction

Light-harvesting (LH) antenna systems used in bacterial photosynthesis are characterized by highly organized arrays of chlorophyll (Chl) pigments. In purple photosynthetic bacteria, circular organization of Chl pigments is achieved through supercomplexation with intrinsic membrane proteins.[1–18] In green photosynthetic bacteria, on the other hand, the self-assembly of specifically evolved self-aggregative Chls ("chlorosomal" Chls) enables the construction of tubular mesoscale structures without the need for protein scaffolding in extramembranous LH apparatuses.[19–25] The self-assembly is driven by the concerted action of a variety of noncovalent interactions. Mimicking these highly organized arrays of naturally-occurring pigments through synthetic supramolecular dye chemistry not only provides insights into structure–property correlations but also paves the way for using these naturally-abundant π-conjugated molecules as active materials in optoelectronic devices.[25–27]

In synthetic systems, self-assembly of metallochlorins designed based on the structures of chlorosomal Chls has been investigated in both organic solvents and aqueous solutions.[28–41] These chlorins formed nanotubes through the concerted action of hydrogen bonds, coordination bonds, π–π stacking and van der Waals interactions. Although nanotubes are formed through non-hierarchical processes, from a topolo-

[a]*Division of Advanced Science and Engineering, Graduate School of Engineering, Chiba University, 1-33 Yayoi-cho, Inage-ku, Chiba 263-8522, Japan*
[b]*Department of Applied Chemistry and Biotechnology, Graduate School of Engineering, Chiba University, 1-33 Yayoi-cho, Inage-ku, Chiba 263-8522, Japan. E-mail: yagai@faculty.chiba-u.jp*
[c]*Department of Chemistry, Faculty of Engineering and Technology, SRM Institute of Science and Technology, Kattankulathur, Chengalpattu 603 203, Tamil Nadu, India*
[d]*Graduate School of Life Sciences, Ritsumeikan University, Kusatsu, Shiga 525-8577, Japan*
[e]*Department of Chemistry, College of Humanities & Sciences, Nihon University, Setagaya-ku, Tokyo 156-8550, Japan*
[f]*ISIS Pulsed Neutron Source, Rutherford Appleton Laboratory, Didcot, OX11 0QX, UK*
[g]*Department of Chemistry, School of Chemical and Physical Sciences, Keele University, Keele, Staffordshire ST55BG, UK*
[h]*Center for Basic Research on Materials, National Institute for Materials Science, 1-1 Namiki, Tsukuba, Ibaraki 305-0044, Japan*
[i]*Research Center for Autonomous Systems Materialogy (ASMat), Institute of Integrated Research, Institute of Science Tokyo, 4259 Nagatsuda-cho, Midori-ku, Yokohama, Kanagawa 226-8501, Japan*
[j]*Institute for Advanced Academic Research (IAAR), Chiba University, 1-33 Yayoi-cho, Inage-ku, Chiba 263-8522, Japan*

†Electronic supplementary information (ESI) available: General information, synthesis, structural characterization data, photophysical, morphological, small-angle X-ray and neutron scattering studies and their model fittings. See DOI: https://doi.org/10.1039/d4qo01629g

gical perspective, slicing these nanotubes yields ring structures.[42] Conversely, from the viewpoint of hierarchical self-assembly, stacking rings results in the formation of nanotubes. Therefore, by designing circular supramolecular assembly and controlling their hierarchical stacking, both ring and tube structures can be created.

We herein report the construction of circular and tubular assemblies of synthetic Chl-*a* derivatives by hierarchical assembly control of the similar supramolecular motif. We have previously demonstrated that by modifying π-conjugated molecules with barbituric acid and a tri(dodecyloxy)phenyl (minidendron) units,[43] supramolecular polymers can be constructed through the formation of hydrogen-bonded cyclic hexamers (rosettes) and their hierarchical stacking.[44–49] In order to obtain discrete and stackable rosettes of Chl-*a* derivatives, we synthesized a series of barbituric-acid-functionalized chlorins **ChG2** and **ChG3**, modified with Percec-type dendrons[43] of different bulkiness: second- (G2) and third-generation (G3) dendrons (Fig. 1). **ChG2** formed supramolecular nanofibers of stacked rosettes, while **ChG3** only assembled to rosette level.

## Results and discussion

Free base chlorins **ChG2** and **ChG3** were synthesized following Scheme S1 (in the ESI†). These compounds were characterized by $^{1}$H and $^{13}$C NMR spectroscopies and ESI mass spectrometry. To study the rosette formation, we measured concentration-dependent $^{1}$H NMR spectra of **ChG2** and **ChG3** (Fig. S1†). At submillimolar concentrations (*e.g.*, 0.1 mM), two sharp signals corresponding to the N–H protons ($H_{syn}$ and $H_{anti}$) of the barbituric acid unit appeared around 8.1 ppm for both the molecules. As the concentration increased to 20 mM, these two N–H signals gradually shifted downfield, indicating hydrogen-bonding. The difference in downfield shifts, $\Delta(\delta_{syn} - \delta_{anti})$, between $H_{syn}$ and $H_{anti}$ reached 0.29 ppm for **ChG2** and 0.27 ppm for **ChG3** at 20 mM, respectively (Fig. S2†). This result is characteristic of rosette formation where the two N–H protons experience different deshielding environments.[49]

Next, we studied self-assembly of **ChG2** and **ChG3** in methylcyclohexane (MCH), a nonpolar solvent, by using variable-temperature (VT) UV/Vis and circular dichroism (CD) spectroscopies (Fig. 2). The UV/Vis spectrum of **ChG2** ($c$ = 10 μM) at 100 °C showed Soret and Qy absorption maxima at 386 and 713 nm, respectively (Fig. 2a, upper). Upon cooling to 20 °C at a rate of 1 °C min$^{-1}$, these peaks shifted hypsochromically to 362 and 698 nm. The spectral change indicates that the chlorin chromophore stacks in a face-to-face (H-type) arrangement. Plotting the UV/Vis absorption change at 386 nm against temperature revealed a non-sigmoidal aggregation curve (Fig. S3a,† blue line). Upon heating at a rate of 1 °C min$^{-1}$, the plot showed significant thermal hysteresis, suggesting that the cooling process is not under thermodynamic control. This was further supported by retardation of nucleation upon increasing cooling rate (Fig. S4†).[50] These results indicated that **ChG2** exhibits cooperative supramolecular polymerization involving nucleation followed by elongation processes.[51] In the VT-CD measurements, the growth of a strong Cotton effect was observed in the Soret region upon cooling, while the Qy band showed a weak Cotton effect (Fig. 2a, lower). These CD signals are in good agreement with the face-to-face stacking of the entire chlorin chromophores, which is different from aggregation of chlorosomal Chls along to their Qy axes. In sharp contrast, UV/Vis and CD spectra of **ChG3** displayed only marginal changes upon cooling even at a much higher concentration of 150 μM (Fig. 2b). Temperature-dependence of the absorption spectra are unlikely those recorded for aggregation and dissociation, and no significant thermal hysteresis was observed upon heating at a rate of 1 °C

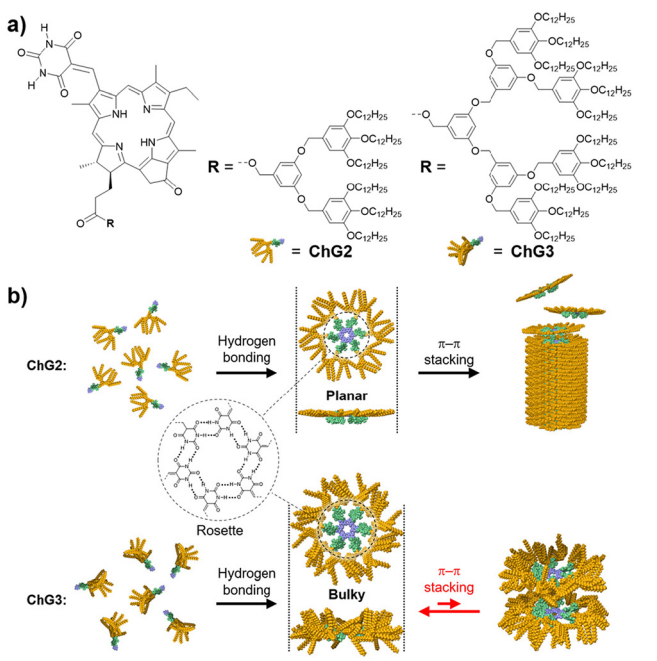


**Fig. 1** (a) Molecular structures of **ChG2** and **ChG3**. (b) Schematic representation showing the self-assembly of **ChG2** and **ChG3** into columnar and discrete aggregates.

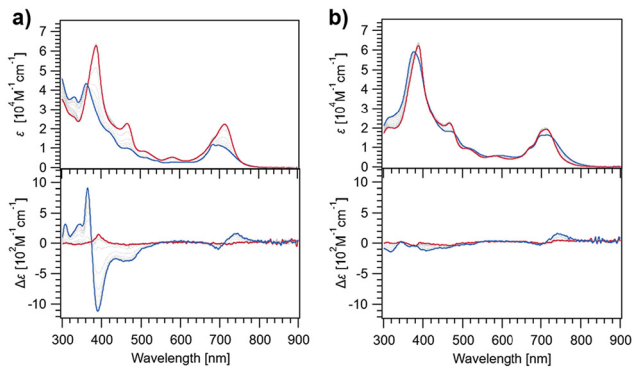


**Fig. 2** UV/Vis (upper) and CD absorption spectra (lower) of **ChG2** (a) and **ChG3** (b) in MCH at 100 °C (red lines) and 20 °C (blue lines). (Concentration: **ChG2** = 10 μM, **ChG3** = 150 μM.)

min$^{-1}$ (Fig. S3b†). The entirely different temperature-dependence of **ChG2** and **ChG3** implies their distinct self-organization behaviors.

The formation of extended fibrous structures by **ChG2** and small species by **ChG3** was demonstrated by small-angle X-ray and neutron scattering (SAXS/SANS) experiments in MCH-$d_{14}$ (Fig. 3). Analysis of the combined datasets for each solution, using a model representing a core–shell cylinder with globally constrained assembly dimensions, was performed using SasView,[52] as detailed in the ESI.† The SAXS/SANS data for a solution of **ChG2** is indicative of elongated fibers, with length, $L \geq 100$ nm, aromatic core radius, $R_{core} = 2.6 \pm 0.1$ nm and *n*-alkyl shell thickness, $\delta_{shell} = 1.2 \pm 0.1$ nm (Fig. 3a and c). This gives a fiber diameter of 7.6 ± 0.2 nm, in line with the diameter of the **ChG2** rosette estimated by molecular modelling calculations (Fig. S5†). There is good agreement between SAXS/SANS data and the model for much of the *Q*-range. However, maximum at $Q \sim 0.28$ Å$^{-1}$ is visible in the SAXS that is not apparent in the SANS and unaccounted for in the analysis. While we are presently unable to definitively explain this phenomenon, its possible origin is suggested in the ESI.† The SAXS/SANS data for a solution of **ChG3** is quite different to that for **ChG2** (Fig. 3b and d). The SANS data exhibits a flat $I(Q) \sim Q^{0}$ region at low *Q* on the log–log plot and therefore indicates far less elongated assembly structures in solution. Combined SAXS/SANS analysis gave $R_{core} = 3.1 \pm 0.1$ nm, $\delta_{shell} = 1.1 \pm 0.1$ nm and $L = 2.1 \pm 0.1$ nm. This supports the existence of rosettes of **ChG3** in solution but suggests that, unlike **ChG2**, they do not extensively stack—in line with the UV/Vis and CD findings. The upturn in $I(Q)$ at low *Q* in the SAXS data for **ChG3** may suggest some localised aggregation or limited stacking of a small number of rosettes, which may explain the slight differences before and after cooling noted in Fig. 2b.

Highly extended nanofibers were imaged for self-assembled **ChG2** by atomic force microscopy (AFM) and transmission electron microscopy (TEM) (Fig. 4). In the AFM images acquired for spin-coated samples, right-handed helical structures with a helical pitch of 9.5 nm are observed (Fig. 4a, b and S6†). The right-handed helicity indicates clockwise rotation of the **ChG2** rosette upon stacking. On the other hand, TEM imaging of drop-cast samples visualized both isolated individual nanofibers and also dense arrays of bundled nanofibers (Fig. 4c, e and S7†). This finding could be attributed to a concentration gradient during a slow drying process of solvent after drop casting, which was confirmed by concentration-dependent AFM images (Fig. S8†). For the isolated nanofibers, the visible width was measured to be approximately 5.1 nm (Fig. 4c and d). This value is very similar to the diameter of the π-conjugated core ($2R_{core} = 5.2$ nm) indicated by SAXS/SANS analysis. For the bundled nanofibers, their long-range ordering with a periodicity of 6.8 nm was observed (Fig. 4e and f). This value is smaller than the diameter of solvated nanofibers (7.6 nm) shown by SAXS/SANS analysis, suggesting that the alkyl chains are tightly packed or interdigitated between nanofibers on the substrate.

In stark contrast, uniform small particles with heights of 2–3 nm and widths of 7–8 nm were imaged for **ChG3** by AFM

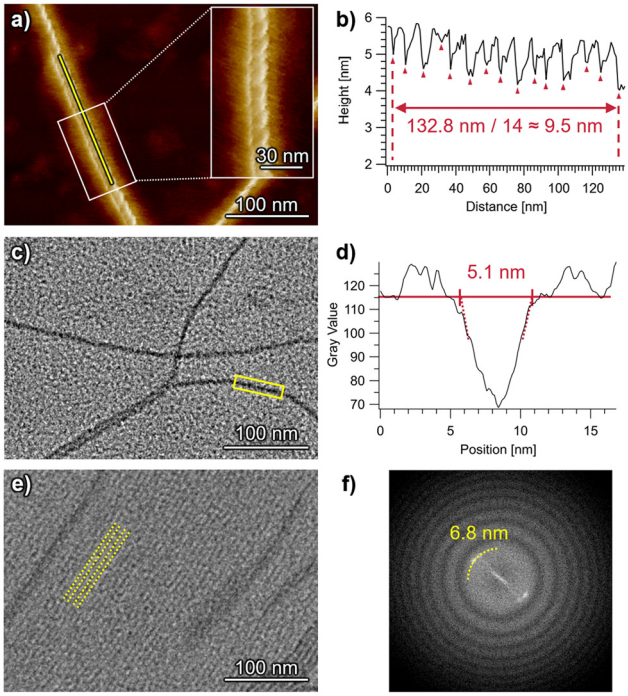


**Fig. 4** (a) AFM image of aggregates spin-coated immediately after cooling an MCH solution of **ChG2** (10 μM) from 100 °C to 20 °C at a rate of 1 °C min$^{-1}$. The inset image is magnified view. (b) AFM height analysis of a fiber formed by **ChG2** (along the yellow line in a). (c and e) TEM images of **ChG2** (30 μM) drop-casted on an amorphous carbon film. (c) TEM image of an individual and bundled fibers. (d) Intensity profile of the selected area in c (yellow box). The horizontal line (red) corresponds to gray value of the image background. (e) TEM image of aligned fibers. Yellow dotted lines indicate fiber orientation and spacing. (f) Fast Fourier transform pattern corresponding to (e), showing the signal assignable to the interfiber spacing of 6.8 nm.

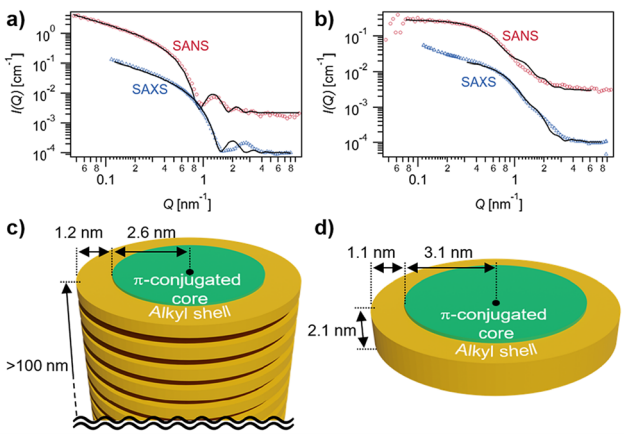


**Fig. 3** (a and b) SANS (red circles) and SAXS (blue triangles) data of **ChG2** (a) and **ChG3** (b) in MCH-$d_{14}$ (*c* = 300 μM). Black solid lines represent fits of the data. The scattered intensity, $I(Q)$, is plotted as a function of the scattering vector, *Q*. (c and d) Schematic illustrations of assemblies of **ChG2** (c) and **ChG3** (d).

(Fig. 5 and S9†), corresponding to the dimension of the height (2.1 nm) and diameter (8.4 nm) of the rosette indicated by SAXS/SANS analysis. Additionally, TEM imaging of the spin-coated samples revealed particles with a smallest width of approximately 6 nm (Fig. 5e and f), corresponding to the diameter of the π-conjugated core ($2R_{core}$ = 6.2 nm) as indicated by SAXS/SANS. This dimension closely matches that of a single **ChG3** rosette in TEM simulation (Fig. S10†). These analyses corroborate that **ChG3** rosette indeed exists as discrete species, likely due to the bulky G3 dendrons inhibiting the stacking of chlorin moieties.

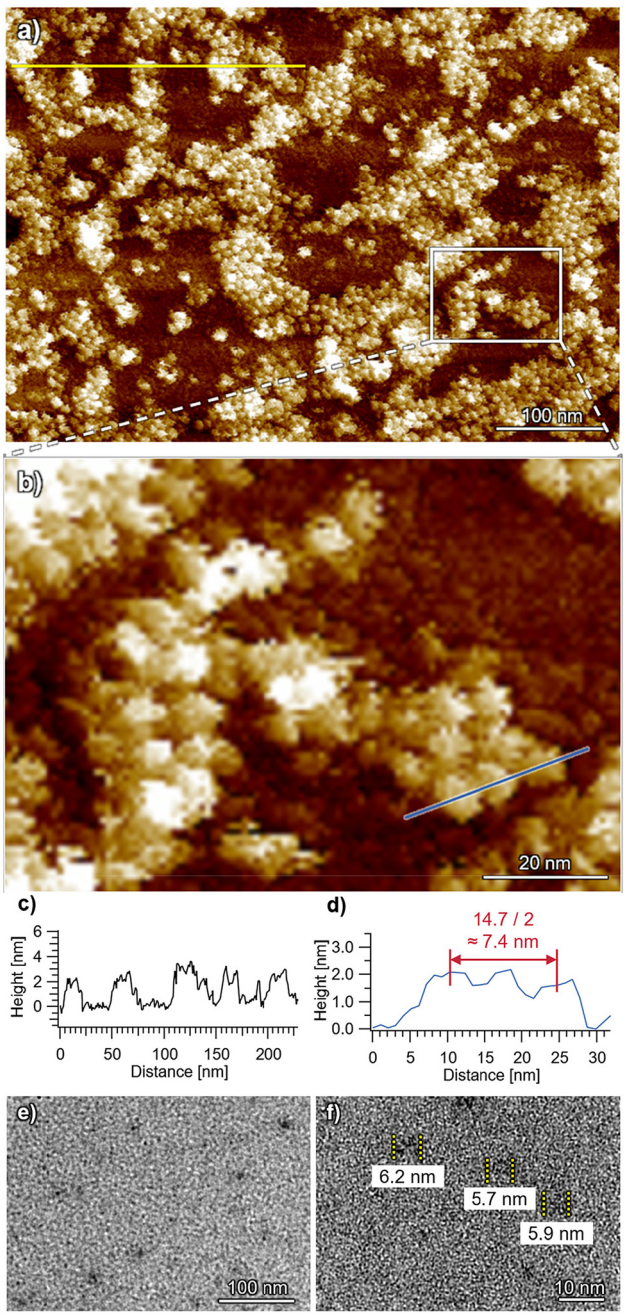


**Fig. 5** (a and b) AFM images of aggregates spin-coated immediately after cooling an MCH solution of **ChG3** (150 μM) from 100 °C to 20 °C at a rate of 1 °C $min^{-1}$. (c and d) AFM cross-sectional analysis of particles formed by **ChG3** along the yellow line in (a) and the blue line in (b), respectively. (e) TEM images of **ChG3** particles on an amorphous carbon film. (f) High-magnification TEM image showing individual **ChG3** particles.

## Conclusions

While Chl nanotubes have been the subject of numerous studies, there has been limited exploration into the cross-sectional counterpart, *i.e.*, circular assemblies that can hierarchically assemble into nanotubes. Our present research focused on engineering circular assemblies of Chl pigments using the hydrogen-bonding capability of barbituric acid. These circular assemblies tend to stack into tubular structures; however, by altering the bulkiness of surrounding alkyl side chains, we have effectively distinguished between the formation of circular and tubular assemblies. This approach enables precise control over the hierarchical organization of molecular assemblies with similar motifs, allowing for an unbiased comparison of their structural and functional properties. Investigating the optical characteristics of these ring and tube structures may provide crucial insights into the evolutionary importance of Chl's light-harvesting mechanism in photosynthesis, and pave the way for future applications.

## Author contributions

Conceptualization, R. K., S. Y.; resources, H. T., N. H.; investigation, data curation, formal analysis except for SAXS/SANS and TEM, R. K.; investigation of SANS, S. R.; investigation of SANS, data curation and formal analysis of SAXS/SANS, M. H., H. H.; investigation, data curation, formal analysis of TEM, B. M., K. H.; all authors prepared and edited the overall manuscript including figures; funding acquisition, H. T., S. Y.; supervision, S. Y. All authors have read and agreed to the final version of the manuscript.

## Data availability

The data that support the findings of this work have been included in the main text and ESI.†

## Conflicts of interest

Authors declare no conflicts of interest.

## Acknowledgements

This work was supported by the Japan Society for the Promotion for Science (JSPS) KAKENHI grant no. JP22H00331, JP22H02203, JP23H04874 and JP23H04873 in a Grant-in-Aid

for Transformative Research Areas "Materials Science of Meso-Hierarchy". B. V. thanks the JSPS for research fellowship P1934. This work was performed under the approval of the Photon Factory Program Advisory Committee (Proposal No. 2022G537). The authors are grateful to Dr Nobutaka Shimizu, Dr Hideaki Takagi, and Dr Rie Haruki for the measurements of SAXS. This work benefited from the use of the SasView application, originally developed under NSF award DMR-0520547. SasView contains code developed with funding from the European Union's Horizon 2020 research and innovation programme under the SINE2020 project, grant agreement No. 654000.



## References

1 G. McDermott, S. M. Prince, A. A. Freer, A. M. Hawthornthwaite-Lawless, M. Z. Papiz, R. J. Cogdell and N. W. Isaacs, Crystal structure of an integral membrane light-harvesting complex from photosynthetic bacteria, *Nature*, 1995, **374**, 517.

2 T. Pullerits and V. Sundström, Photosynthetic Light-Harvesting Pigment-Protein Complexes: Toward Understanding How and Why, *Acc. Chem. Res.*, 1996, **29**, 381.

3 H. Lokstein, G. Renger and J. P. Götze, Photosynthetic Light-Harvesting (Antenna) Complexes—Structures and Functions, *Molecules*, 2021, **26**, 3378.

4 Y. Kimura, K. Tani, M. T. Madigan and Z.-Y. Wang-Otomo, Advances in the Spectroscopic and Structural Characterization of Core Light-Harvesting Complexes from Purple Phototrophic Bacteria, *J. Phys. Chem. B*, 2023, **127**, 6.

5 K. Timpmann, L. Kangur and A. Freiberg, Hysteretic Pressure Dependence of $Ca^{2+}$ Binding in LH1 Bacterial Membrane Chromoproteins, *J. Phys. Chem. B*, 2023, **127**, 456.

6 X.-L. Liu, Y.-Y. Hu, K. Li, M.-Q. Chen and P. Wang, Reconstituted LH2 in multilayer membranes induced by poly-L-lysine: Structure of supramolecular and electronic states, *Arabian J. Chem.*, 2023, **16**, 104600.

7 Y. Saga, K. Hamanishi, T. Yamamoto, K. Hinago and Y. Nagasawa, Conversion of B800 Bacteriochlorophyll *a* to 3-Acetyl Chlorophyll *a* in the Light-Harvesting Complex 3 by *In Situ* Oxidation, *J. Phys. Chem. B*, 2023, **127**, 2683.

8 L. Bracun, A. Yamagata, B. M. Christianson, M. Shirouzu and L.-N. Liu, Cryo-EM structure of a monomeric RC-LH1-PufX supercomplex with high-carotenoid content from *Rhodobacter capsulatus*, *Structure*, 2023, **31**, 318.

9 A. Hitchcock, D. J. K. Swainsbury and C. N. Hunter, Photosynthesis in the near infrared: the γ subunit of *Blastochloris viridis* LH1 red-shifts absorption beyond 1000 nm, *Biochem. J.*, 2023, **480**, 455.

10 K. Otomo, T. Dewa, M. Matsushita and S. Fujiyoshi, Cryogenic Single-Molecule Fluorescence Detection of the Mid-Infrared Response of an Intrinsic Pigment in a Light-Harvesting Complex, *J. Phys. Chem. B*, 2023, **127**, 4959.

11 M. Rätsep, A. Lehtmets, L. Kangur, K. Timpmann, K. Leiger, Z.-Y. Wang-Otomo and A. Freiberg, Evaluation of the relationship between color-tuning of photosynthetic excitons and thermodynamic stability of light-harvesting chromoproteins, *Photosynthetica*, 2023, **61**, 308.

12 O. Thwaites, B. M. Christianson, A. J. Cowan, F. Jackel, L.-N. Liu and A. M. Gardner, Unravelling the Roles of Integral Polypeptides in Excitation Energy Transfer of Photosynthetic RC-LH1 Supercomplexes, *J. Phys. Chem. B*, 2023, **127**, 7283.

13 K. Timpmann, M. Rätsep and A. Freiberg, Dominant role of excitons in photosynthetic color-tuning and light-harvesting, *Front. Chem.*, 2023, **11**, 1231431.

14 C.-H. Qi, G.-L. Wang, F.-F. Wang, Y. Xin, M.-J. Zou, M. T. Madigan, Z.-Y. Wang-Otomo, F. Ma and L.-J. Yu, New insights on the photocomplex of *Roseiflexus castenholzii* revealed from comparisons of native and carotenoid-depleted complexes, *J. Biol. Chem.*, 2023, **299**, 105057.

15 T. Dewa, K. Kimoto, G. Kasagi, H. Harada, A. Sumino and M. Kondo, Functional Coupling of Biohybrid Photosynthetic Antennae and Reaction Center Complexes: Quantitative Comparison with Native Antennae, *J. Phys. Chem. B*, 2023, **127**, 10315.

16 J.-F. Hao, N. Yamano, C.-H. Qi, Y. Zhang, F. Ma, P. Wang, L.-J. Yu and J.-P. Zhang, Carotenoid-Mediated Long-Range Energy Transfer in the Light Harvesting-Reaction Center Complex from Photosynthetic Bacterium *Roseiflexus castenholzii*, *J. Phys. Chem. B*, 2023, **127**, 10360.

17 C.-H. Qi, G.-L. Wang, F.-F. Wang, J. Wang, X.-P. Wang, M.-J. Zou, F. Ma, M. T. Madigan, Y. Kimura, Z.-Y. Wang-Otomo and L.-J. Yu, Structural insights into the unusual core photocomplex from a triply extremophilic purple bacterium, *Halorhodospira halochloris, J. Integr. Plant Biol.*, DOI: **10.1111/jipb.13628**, in press.

18 Y. Saga, K. Hamanishi and S. Kawato, Removal of B800 Bacteriochlorophyll *a* from Light-Harvesting Complex 3 of the Purple Photosynthetic Bacterium, *Rhodoblastus acidophilus, Plant Cell Physiol.*, DOI: **10.1093/pcp/pcae065**, in press.

19 T. S. Balaban, H. Tamiaki and A. R. Holzwarth, Chlorins programmed for self-assembly, *Top. Curr. Chem.*, 2005, **258**, 1.

20 V. Erić, X. Li, L. Dsouza, S. K. Frehan, A. Huijser, A. R. Holzwarth, F. Buda, G. J. A. Sevink, H. J. M. de Groot and T. L. C. Jansen, Manifestation of Hydrogen Bonding and Exciton Delocalization on the Absorption and Two-Dimensional Electronic Spectra of Chlorosomes, *J. Phys. Chem. B*, 2023, **127**, 1097.

21 V. Erić, J. L. Castro, X. Li, L. Dsouza, S. K. Frehan, A. Huijser, A. R. Holzwarth, F. Buda, G. J. A. Sevink, H. J. M. de Groot and T. L. C. Jansen, Ultrafast Anisotropy Decay Reveals Structure and Energy Transfer in Supramolecular Aggregates, *J. Phys. Chem. B*, 2023, **127**, 7487.

22 S. K. Frehan, L. Dsouza, X. Li, V. Eríc, T. L. C. Jansen, G. Mul, A. R. Holzwarth, F. Buda, G. J. A. Sevink,

 

H. J. M. de Groot and A. Huijser, Photon Energy-Dependent Ultrafast Exciton Transfer in Chlorosomes of *Chlorobium tepidum* and the Role of Supramolecular Dynamics, *J. Phys. Chem. B*, 2023, **127**, 7581.

23 V. Erić, X. Li, L. Dsouza, A. Huijser, A. R. Holzwarth, F. Buda, G. J. A. Sevink, H. J. M. de Groot and T. L. C. Jansen, Observation of Dark States in Two-Dimensional Electronic Spectra of Chlorosomes, *J. Phys. Chem. B*, 2024, **128**, 3575.

24 L. Dsouza, X. Li, V. Erić, A. Huijser, T. L. C. Jansen, A. R. Holzwarth, F. Buda, D. A. Bryant, S. Bahri, K. B. S. S. Gupta, G. J. A. Sevink and H. J. M. de Groot, An integrated approach towards extracting structural characteristics of chlorosomes from a *bchQ* mutant of *Chlorobaculum tepidum*, *Phys. Chem. Chem. Phys.*, 2024, **26**, 15856.

25 S. Matsubara and H. Tamiaki, Supramolecular chlorophyll aggregates inspired from specific light-harvesting antenna "chlorosome": Static nanostructure, dynamic construction process, and versatile application, *J. Photochem. Photobiol., C: Photochem. Rev.*, 2020, **45**, 100385.

26 T. S. Balaban, Tailoring Porphyrins and Chlorins for Self-Assembly in Biomimetic Artificial Antenna Systems, *Acc. Chem. Res.*, 2005, **38**, 612.

27 S. Sengupta and F. Würthner, Chlorophyll J-Aggregates: From Bioinspired Dye Stacks to Nanotubes, Liquid Crystals, and Biosupramolecular Electronics, *Acc. Chem. Res.*, 2013, **46**, 2498.

28 H. Tamiaki, M. Amakawa, Y. Shimono, R. Tanikaga, A. R. Holzwarth and K. Schaffner, Synthetic zinc and magnesium chlorin aggregates as models for supramolecular antenna complexes in chlorosomes of green photosynthetic bacteria, *Photochem. Photobiol.*, 1996, **63**, 92.

29 V. Huber, M. Katterle, M. Lysetska and F. Würthner, Reversible self-organization of semisynthetic zinc chlorins into well-defined rod antennae, *Angew. Chem., Int. Ed.*, 2005, **44**, 3147.

30 T. Miyatake and H. Tamiaki, Self-aggregates of bacteriochlorophylls-*c*, *d* and *e* in a light-harvesting antenna system of green photosynthetic bacteria: Effect of stereochemistry at the chiral 3-(1-hydroxyethyl) group on the supramolecular arrangement of chlorophyllous pigments, *J. Photochem. Photobiol., C: Photochem. Rev.*, 2005, **6**, 89.

31 S. Uemura, S. Sengupta and F. Würthner, Cyclic self-assembled structures of chlorophyll dyes on HOPG by the dendron wedge effect, *Angew. Chem., Int. Ed.*, 2009, **48**, 7825.

32 T. Miyatake and H. Tamiaki, Self-aggregates of natural chlorophylls and their synthetic analogues in aqueous media for making light-harvesting systems, *Coord. Chem. Rev.*, 2010, **254**, 2593.

33 S. Sengupta, S. Uemura, S. Patwardhan, V. Huber, F. C. Grozema, L. D. A. Siebbeles, U. Baumeister and F. Würthner, Columnar mesophases based on zinc chlorophyll derivatives functionalized with peripheral dendron wedges, *Chem. – Eur. J.*, 2011, **17**, 5300.

34 S. Sengupta, D. Ebeling, S. Patwardhan, X. Zhang, H. Vona Berlepsch, C. Böttcher, V. Stepanenko, S. Uemura, C. Hentschel, H. Fuchs, F. C. Grozema, L. D. A. Siebbeles, A. R. Holzwarth, L. Chi and F. Würthner, Biosupramolecular nanowires from chlorophyll dyes with exceptional charge-transport properties, *Angew. Chem., Int. Ed.*, 2012, **51**, 6378.

35 S. Shoji, T. Hashishin and H. Tamiaki, Construction of Chlorosomal Rod Self-Aggregates in the Solid State on Any Substrates from Synthetic Chlorophyll Derivatives Possessing an Oligomethylene Chain at the 17-Propionate Residue, *Chem. – Eur. J.*, 2012, **18**, 13331.

36 S. Shoji, T. Ogawa, T. Hashishin, S. Ogasawara, H. Watanabe, H. Usami and H. Tamiaki, Nanotubes of biomimetic supramolecules constructed by synthetic metal chlorophyll derivatives, *Nano Lett.*, 2016, **16**, 3650.

37 S. Ogi, C. Grzeszkiewicz and F. Würthner, Pathway complexity in the self-assembly of a zinc chlorin model system of natural bacteriochlorophyll J-aggregates, *Chem. Sci.*, 2018, **9**, 2768.

38 A. Löhner, T. Kunsel, M. I. S. Röhr, T. L. C. Jansen, S. Sengupta, F. Würthner, J. Knoester and J. Köhler, Spectral and Structural Variations of Biomimetic Light-Harvesting Nanotubes, *J. Phys. Chem. Lett.*, 2019, **10**, 2715.

39 S. Shoji, V. Stepanenko, F. Würthner and H. Tamiaki, Self-Assembly of a Zinc Bacteriochlorophyll-*d* Analog with a Lipophilic Tertiary Amide Group in the 17-Substituent, *Bull. Chem. Soc. Jpn.*, 2022, **95**, 1083.

40 N. Hara and H. Tamiaki, Temperature-dependent chlorosomal self-aggregation of bacteriochlorophyll-*d* analogs with a branched alkyl chain in a single 1-chlorooctane solvent, *Bull. Chem. Soc. Jpn.*, 2024, **97**, uoae032.

41 A. Toda and H. Tamiaki, Self-aggregation of synthetic zinc bacteriochlorophyll-*d* analogs with pinacol boronates on the B-ring, *J. Photochem. Photobiol., A: Chem.*, 2024, **452**, 115616.

42 T. Fukino, H. Joo, Y. Hisada, M. Obana, H. Yamagishi, T. Hikima, M. Takata, N. Fujita and T. Aida, Interfacial effects in iron-nickel hydroxide-platinum nanoparticles enhance catalytic oxidation, *Science*, 2014, **344**, 499.

43 B. M. Rosen, C. J. Wilson, D. A. Wilson, M. Peterca, M. R. Imam and V. Percec, Dendron-mediated self-assembly, disassembly, and self-organization of complex systems, *Chem. Rev.*, 2009, **109**, 6275.

44 S. Yagai, Y. Kitamoto, S. Datta and B. Adhikari, Supramolecular Polymers Capable of Controlling Their Topology, *Acc. Chem. Res.*, 2019, **52**, 1325.

45 S. Datta, S. Takahashi and S. Yagai, Nanoengineering of Curved Supramolecular Polymers: Toward Single-Chain Mesoscale Materials, *Acc. Mater. Res.*, 2022, **3**, 259.

46 X. Lin, M. Suzuki, M. Gushiken, M. Yamauchi, T. Karatsu, T. Kizaki, Y. Tani, K. I. Nakayama, M. Suzuki, H. Yamada, T. Kajitani, T. Fukushima, Y. Kikkawa and S. Yagai, Hydrogen-bonded rosettes comprising π-conjugated systems as building blocks for functional one-dimensional assemblies, *Sci. Rep.*, 2017, **7**, 43098.

47 B. Adhikari, X. Lin, M. Yamauchi, H. Ouchi, K. Aratsu and S. Yagai, Supramolecular polymerization of hydrogen-bonded rosettes with anthracene chromophores: Regioisomeric effect on nanostructures, *Chem. Commun.*, 2017, **53**, 9663.
48 D. D. Prabhu, K. Aratsu, M. Yamauchi, X. Lin, B. Adhikari and S. Yagai, Supramolecular Polymerization of Supermacrocycles: Effect of Molecular Conformations on Kinetics and Morphology, *Polym. J.*, 2017, **49**, 189.
49 M. Yamauchi, B. Adhikari, D. D. Prabhu, X. Lin, T. Karatsu, T. Ohba, N. Shimizu, H. Takagi, R. Haruki, S. Adachi, T. Kajitani, T. Fukushima and S. Yagai, High-fidelity self-assembly pathways for hydrogen-bonding molecular semiconductors, *Chem. – Eur. J.*, 2017, **23**, 5270.
50 S. Ogi, V. Stepanenko, K. Sugiyasu, M. Takeuchi and F. Würthner, Mechanism of self-assembly process and seeded supramolecular polymerization of perylene bisimide organogelator, *J. Am. Chem. Soc.*, 2015, **137**, 3300.
51 P. Jonkheijm, P. van der Schoot, A. P. H. J. Schenning and E. W. Meijer, Probing the solvent-assisted nucleation pathway in chemical self-assembly, *Science*, 2006, **313**, 80.
52 SasView for Small Angle Scattering Analysis, **https://www.sasview.org/**, (accessed August 2024).